Spectrochimica Acta Part A: Molecular and Biomolecular Spectroscopy 292 (2023) 122403

Contents lists available at ScienceDirect

Spectrochimica Acta Part A: Molecular and Biomolecular Spectroscopy

journal homepage: www.journals.elsevier.com/spectrochimica-acta-part-a-molecular-and-biomolecular-spectroscopy

A novel fluorescence sensor for uranyl ion detection based on a dansyl-modified peptide

Lianshun Zhang [a], Mengqing Jia [a], Xi Wang [a], Lei Gao [b], Bo Zhang [a], Lei Wang [a], Jinming Kong [c], Lianzhi Li [a,*]

[a] School of Chemistry and Chemical Engineering, Liaocheng University, Liaocheng 252059, PR China
[b] Zhong Yuan Academy of Biological Medicine, Liaocheng People's Hospital, Liaocheng 252000, PR China
[c] School of Environmental and Biological Engineering, Nanjing University of Science and Technology, Nanjing, Jiangsu 210094, PR China

HIGHLIGHTS

- A novel dansyl-modified peptide fluorescence sensor was synthesized via Fmoc solid phase peptide synthesis.
- The sensor displayed an excellent selectivity and high sensitivity for UO_2^{2+} detection by turn off fluorescence response.
- The interaction of the sensor with UO_2^{2+} was characterized by ESI-MS, IR, XPS and Time-resolved fluorescence spectroscopy and ITC measurement.
- The sensor showed good practicality for UO_2^{2+} detection in lake water sample.

GRAPHICAL ABSTRACT

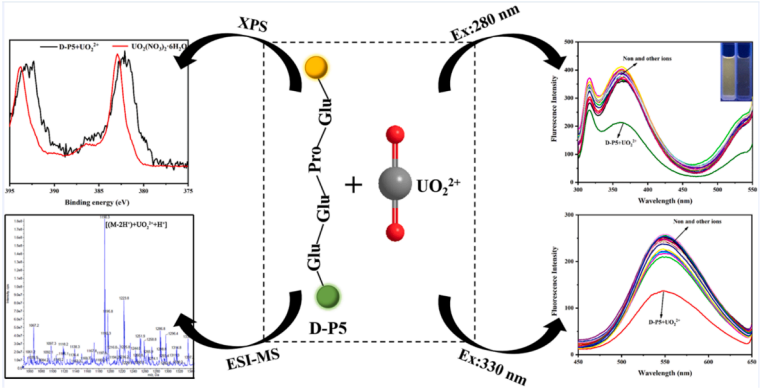

ARTICLE INFO

Keywords:
Dansyl-modified peptide sensor
Fluorescence sensing
Uranyl ion

ABSTRACT

It is of great significance to sensitively and selectively detect uranyl ion (UO_2^{2+}) in environmental and biological samples due to the high risks of UO_2^{2+} to human health. However, such suitable sensors are still scarce. A novel fluorescence sensor based on a dansyl-modified peptide, Dansyl-Glu-Glu-Pro-Glu-Trp-COOH (D-P5), was efficiently synthesized by Fmoc solid phase peptide synthesis. As the first linear peptide-based fluorescence sensor for UO_2^{2+}, D-P5 exhibited high selectivity and sensitivity to UO_2^{2+} over 27 metal ions (UO_2^{2+}, Cr^{3+}, Cu^{2+}, Ba^{2+}, Hg^{2+}, Pb^{2+}, Co^{2+}, Ag^{+}, Fe^{3+}, Ca^{2+}, K^{+}, Mg^{2+}, Mn^{2+}, Na^{+}, Ni^{2+}, Cd^{2+}, Zn^{2+}, Al^{3+}, Dy^{3+}, Er^{3+}, Gd^{2+}, Ho^{3+}, La^{3+}, Lu^{3+}, Pr^{3+}, Sm^{3+}, Tm^{3+}) by a turn-off fluorescence response in 10 mM HEPES buffer (pH 6.3). The effects of anions such as S^{2-}, NO_3, SO_4^{2-} CO_3^{2-}, $HCOO^{-}$, antioxidant ascorbic acid and 4-nitrophenyl acetate on the selectivity for UO_2^{2+} detection were also studies. D-P5 sensor could be used for detecting UO_2^{2+} in a good linear relationship with concentration in the range of 0–8.0 μM with a low limit of detection of 83.2 nM. Furthermore, the interaction of the sensor with UO_2^{2+} was characterized by ESI-MS, IR, XPS and ITC measurements. The 1:1 binding stoichiometry between the sensor and UO_2^{2+} was measured by the job's plot and further verified by ESI-MS. The binding constant of the sensor with UO_2^{2+} was calculated to be 9.8×10^4 M^{-1} by modified Benesi-

* Corresponding author.
E-mail address: lilianzhi1963@163.com (L. Li).

https://doi.org/10.1016/j.saa.2023.122403
Received 30 July 2022; Received in revised form 6 January 2023; Accepted 20 January 2023
Available online 25 January 2023

Hildebrand equation. ITC results showed that the ΔH^{θ} and ΔS^{θ} for the interaction of D-P5 with UO_2^{2+} were −(7.167 ± 1.25) kJ·mol^{-1} and 66.5 J·mol^{-1}·K^{-1}, respectively. Time-resolved fluorescence spectroscopy indicated that the mechanism of fluorescence quenching of D-P5 by UO_2^{2+} ion was static quenching process. In addition, this sensor displayed a good practicality for UO_2^{2+} detection in lake water sample without tedious sample pretreatment.

1. Introduction

Uranium is located in the f-block of the periodic table and belongs to the actinide series [1]. Among various isotopes of uranium, U-235 is used as the fuel for nuclear power generation [2]. In this process, approximately 10^{-5}-10^{-3} M uranium and other radioactive elements will be released. Uranium is radioactive and chemically toxic, which is harmful to animals, plants and humans [3]. When uranium is enriched in the human body, it will cause damage to human bones and kidneys [4]. UO_2^{2+} is one of the main forms of uranium in water solution. Therefore, it is of great importance to develop highly specific and sensitive analytical methods for the detection of UO_2^{2+} ion [5,6]. Currently, some methods have been used to detect uranyl ion including atomic absorption spectrometry [7], inductively coupled plasma mass spectroscopy [8], ion chromatography [9], etc. Although these methods have high sensitivity and low detection limits, they require expensive equipment and complicated sample pretreatments. Fluorescence spectroscopy is a simple and convenient method with many advantages such as good selectivity, high sensitivity, fast response, low detection limit and strong anti-interference ability. Many fluorescent sensors for detection of toxic metal ions such as Hg^{2+}, Al^{3+} and Ag^{+} have been reported [10–12]. Until now, organic molecule fluorescence sensors with Schiff base, carboxylic acid, porphyrin, trimetazidine, tetraphenylethene film etc., have been developed for detecting UO_2^{2+} [13–18]. Although some of them have been successfully applied to the detection of UO_2^{2+}, most of them exhibited the shortcoming of low water solubility, resulting in aggregation and fluorescence quenching. Therefore, it is important to develop a novel uranyl detection method.

Recently, peptide-based fluorescent sensors for metal ion detection have attracted considerable attention due to their good water solubility, biocompatibility, and low toxicity, and thus have important applications in environmental monitoring and bioanalysis [19]. UO_2^{2+} is one of the more stable forms in aqueous solution and under physiological conditions [20], which is a linear *trans*-dioxo cationic structure [21], which is classified as a hard Lewis acid. According to the hard soft acids and bases (HSAB) principle [22], –COOH and $–NH_2$ groups have the tendency to coordinate with it. –COOH is a hard oxygen donor and is suitable for combining with UO_2^{2+} [23,24]. Peptides are composed of various amino acids, and among which, aspartic acid (Asp) and glutamic acid (Glu) can be used as carboxyl donors. Previous study confirmed that peptides containing the two amino acids have high binding ability to UO_2^{2+} [25]. However, only few studies on the binding of peptide with UO_2^{2+} have been reported. Le Clainche et al used a fragment peptide from the first calcium binding site in the paramecium calmodulin as a template to design and synthesize a peptide containing 33 amino acid residues CaM-M3c: EQAEFKEAFAALCTKDGTGTITTKELGTCMRSL [26], which had a specific and strong binding ability to UO_2^{2+}. Although this fragment peptide has some advantages, its disadvantages do exist, its peptide chain is long and difficult to synthesize. In order to overcome those disadvantages, the model peptides DAHK and GGH were synthesized and the binding properties to UO_2^{2+} were study. For these model peptides, they have the advantage of easy synthesis due to the short peptide chain, but the disadvantage is that their binding ability to UO_2^{2+} is weak and cannot specifically recognize UO_2^{2+} ion. DAHK and GGH displayed binding ability not only to UO_2^{2+} but also to Cu^{2+} [27,28]. Therefore, specific recognition of uranyl ion in the presence of competition ions remains a big challenge. To overcome problems for the sophisticated synthesis of protein fragment peptide and the weak and non-specific binding ability to UO_2^{2+} of model peptides, several cyclic peptides have been investigated and showed the promising binding with uranyl ion, which were used as fluorescent sensors for the detection of uranyl ion [21,25]. However, to the best of our knowledge, report on the linear peptidyl fluorescence sensor for detection of UO_2^{2+} remains rare.

In this study, we synthesized a novel linear peptidyl fluorescence sensor Dansyl-Glu-Glu-Pro-Glu-Trp-COOH (D-P5), in which the peptide was modified by a fluorescent dansyl group at the *N*-terminus (Scheme S1). Dansyl chloride is a strong fluorescent agent commonly used in the modification of peptide and protein. It can react specifically with primary amino groups in both aliphatic and aromatic amines to produce a stable and strong blue- or blue-green-fluorescent sulfonamide adduct of dansyl-peptide. For the mechanism, it is obviously different from the detection of UO_2^{2+} by cyclic peptides. In this sensor, fluorescent dansyl group and tryptophan residue can concurrently trigger turn-off fluorescence response by adding UO_2^{2+}, and UO_2^{2+} can be detected at the excitation wavelength of the two fluorescent groups. Compared with the organic molecular sensors, this sensor has better water solubility, biocompatibility and low toxicity, being detected in aqueous solution, and has higher selectivity and sensitivity. The sensor exhibited high selectivity and sensitivity to UO_2^{2+} with a low detection limit. In addition, compared with protein fragment peptide and cyclic peptide, the synthesis process of linear peptide is simpler. To our knowledge, this is the first report on the fluorescent detection of UO_2^{2+} by a linear peptide, which provides a new idea for developing a more powerful biocompatible UO_2^{2+} sensor.

2. Experimental section

2.1. Materials and instruments

Fmoc-Glu(OtBu)–OH, Fmoc-L-Pro-OH, Fmoc-Trp(Boc)–OH and Wang Resin (loading: 0.71 mmol/g) were purchased from CS Bio (Shanghai) ltd. (Shanghai, China). Dansyl chloride was bought from Shanghai Yuanye Bio-Technology Co., ltd. (Shanghai, China). Other chemical reagents such as trifluoroacetic acid (TFA), triisopropylsilane (TIS), N,*N*-diisopropylethylamine and 2-(1H-benzotriazole-1-yl)-1,1,3,3- tetramethyluronium hexafluorophosphate were obtained from Shanghai Macklin Biochemical Co., ltd. (Shanghai, China). Acetonitrile, piperidine, dichloromethane, methanol, ethanol, diethyl ether and N,*N*-dimethylformamide were purchased from commercial suppliers. The stock solutions of 10 mM various metal ions including UO_2^{2+}, Pb^{2+}, Ag^{+}, Cu^{2+}, Ni^{2+}, Dy^{3+}, Er^{3+}, Gd^{2+}, Ho^{3+}, La^{3+}, Lu^{3+}, Pr^{3+}, Sm^{3+} and Tm^{3+} were prepared from their nitrate salts, and Cr^{3+}, Ba^{2+}, Hg^{2+}, Co^{2+}, Fe^{3+}, Ca^{2+}, K^{+}, Mg^{2+}, Mn^{2+}, Na^{+}, Cd^{2+}, Zn^{2+} and Al^{3+} were prepared from their chloride salts. The stock solutions of 10 mM different anion ions including $S_2O_3^{2-}$, S^{2-}, CN^{-}, SO_4^{2-}, NO_3^{-}, HSO_4^{-}, HCO_3^{-}, $HCOO^{-}$, CH_3COO^{-} were prepared from their sodium salt, and CrO_4^{2-} were prepared from its sylvite, ascorbic acid and 4-Nitrophenyl acetate. The above-mentioned salts were purchased from Aladdin Reagent Co. ltd. (Shanghai, China) and from commercial suppliers. 2-[4-(2-hydroxyethyl)piperazin-1-yl] ethanesulfonic acid were purchased from Shanghai Bidepharm Co., ltd. (Shanghai, China). All the solutions used were prepared in 10 mM 2-[4-(2-hydroxyethyl)piperazin-1-yl]ethanesulfonic acid (HEPES) buffer solution at pH 6.3.

CS 136 Peptide Synthesizer (CS Bio Co., USA), Himac-CR22G II high speed refrigerated centrifuge (Hitachi, Japan), API 4500 QTRAP Mass Spectrometer (Applied Biosystems/MDS SCIEX, USA), Hitachi F-7100 fluorescence spectrofluorometer (Hitachi Inc., Japan), FLS 1000 Photoluminescence Spectrometer (UK), ESCALAB Xi^{+} X-

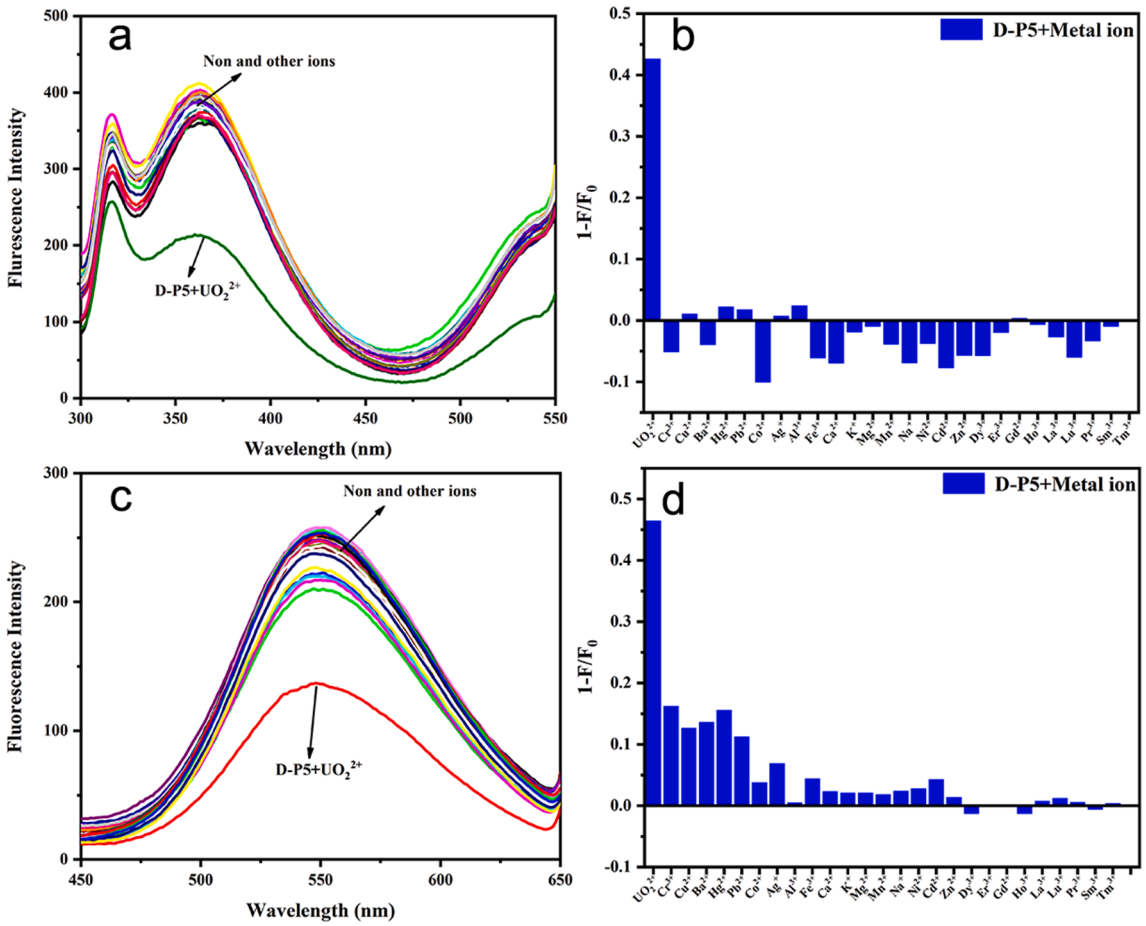

Fig. 1. The fluorescence spectra and fluorescence responses of D-P5 in the presence of 27 metal ions, λex = 280 nm (a,b), λex = 330 nm (c, d). D-P5 concentration was 10 μM, metal ions concentrations were 20 μM.

ray photoelectron spectroscopy (XPS, Thermo Fisher Scientific, NEXSA, USA). Peaks from all of the high-resolution core spectra were fitted with Avantage 5.9 software. The structural information of the samples was measured by Nicolet 6700 Fourier transformation infrared spectrometer (FI-IR) (Nicolet 6700, Thermo Electron Co., USA) using the standard kalium bromatum disk method at wavelengths from 4000 cm^{-1} to 500 cm^{-1}. MicroCal ITC200 titration calorimeter (Microcal, GE Healthcare, UK). Inductively Coupled Plasma Mass Spectrometry (ICP-MS) (ICAP RQ, ThermoFisher Scientific).

2.2. Synthesis of D-P5

The synthesis of D-P5 was performed on a CS136 solid phase peptide synthesizer by using standard Fmoc solid-phase peptide synthesis method. According to the peptide sequence of Dansyl-Glu-Glu-Pro-Glu-Trp-COOH (D-P5), the Fmoc-amino acids (1.5 mmol) were sequentially coupled to the Wang resin (0.5 mmol) from the C-terminus to the *N*-terminus. After deprotecting the Fmoc group, 0.4046 g (1.5 mM) dansyl chloride was added. The formed peptide and protecting groups were cleaved from the resin with 12 mL TFA-TIS-H_2O solution (95:2.5:2.5, v/v/v) for 3.5 h under ambient temperature [29]. The product was filtered in ether at −20 ℃ and centrifuged at −4 ℃ for 5 min with 10000 rpm.

2.3. Fluorescence spectroscopic measurements

A stock solution of 10 mM D-P5 was prepared in 10.0 mM HEPES buffer (pH 6.3). Fluorescence spectra were measured using a Hitachi F-7100 fluorescence spectrofluorometer. Fluorescence spectra of D-P5 in the absence and presence of different metal ions (UO_2^{2+}, Pb^{2+}, Ag^{+}, Cu^{2+}, Ni^{2+}, Dy^{3+}, Er^{3+}, Gd^{2+}, Ho^{3+}, La^{3+}, Lu^{3+}, Pr^{3+}, Sm^{3+} and Tm^{3+} as nitrate salts, Cr^{3+}, Ba^{2+}, Hg^{2+}, Co^{2+}, Fe^{3+}, Ca^{2+}, K^{+}, Mg^{2+}, Mn^{2+}, Na^{+}, Cd^{2+}, Zn^{2+} and Al^{3+} as chloride salts) were measure. In addition, fluorescence spectra of D-P5 in the absence and presence of different anion ions ($S_2O_3^{2-}$, S^{2-}, CN^{-}, SO_4^{2-}, NO_3^{-}, HSO_4^{-}, CrO_4^{2-}, HCO_3^{-}, $HCOO^{-}$, CH_3COO^{-}), antioxidant (ascorbic acid) and nitroaromatic (4-Nitrophenyl acetate) were recorded. All the fluorescence spectra were measured at the excitation wavelength of 280 nm and 330 nm, respectively. Excitation and emission slits were 5 nm and 10 nm, respectively, and the scanning speed was 1200 nm·min^{-1}.

2.4. Determination of binding stoichiometry and binding constant for D-P5 with UO_2^{2+}

The stoichiometric ratio of D-P5 and UO_2^{2+} was determined by the Job's plot method. The fluorescence measurement of the Job's plot was carried out in 10 mM HEPES buffer (pH 6.3). The concentration of D-P5 decreased and the concentration of UO_2^{2+} increased according to the gradient, and the total concentration of both D-P5 and UO_2^{2+} was 20 μM.

The binding constant of D-P5 with UO_2^{2+} was calculated by the modified Benesi-Hildebrand equation:

$$\Delta FI_{max}/\Delta FI = 1 + M^{-n}/K$$

wherein, $\Delta FI_{max} = FI_{max} - FI_0$, $\Delta FI = FI_x - FI_0$, FI_{max} is the maximum fluorescence intensity of D-P5 in the presence of UO_2^{2+} at complete binding state, FI_0 and FI_x refer to the fluorescence intensity of D-P5 and D-P5 in the presence of different concentrations of UO_2^{2+}, respectively. [*M*] is the concentration of UO_2^{2+} and *n* is the number of UO_2^{2+} ion bound to each D-P5 (here $n = 1$), while *K* is the binding constant [30,31].

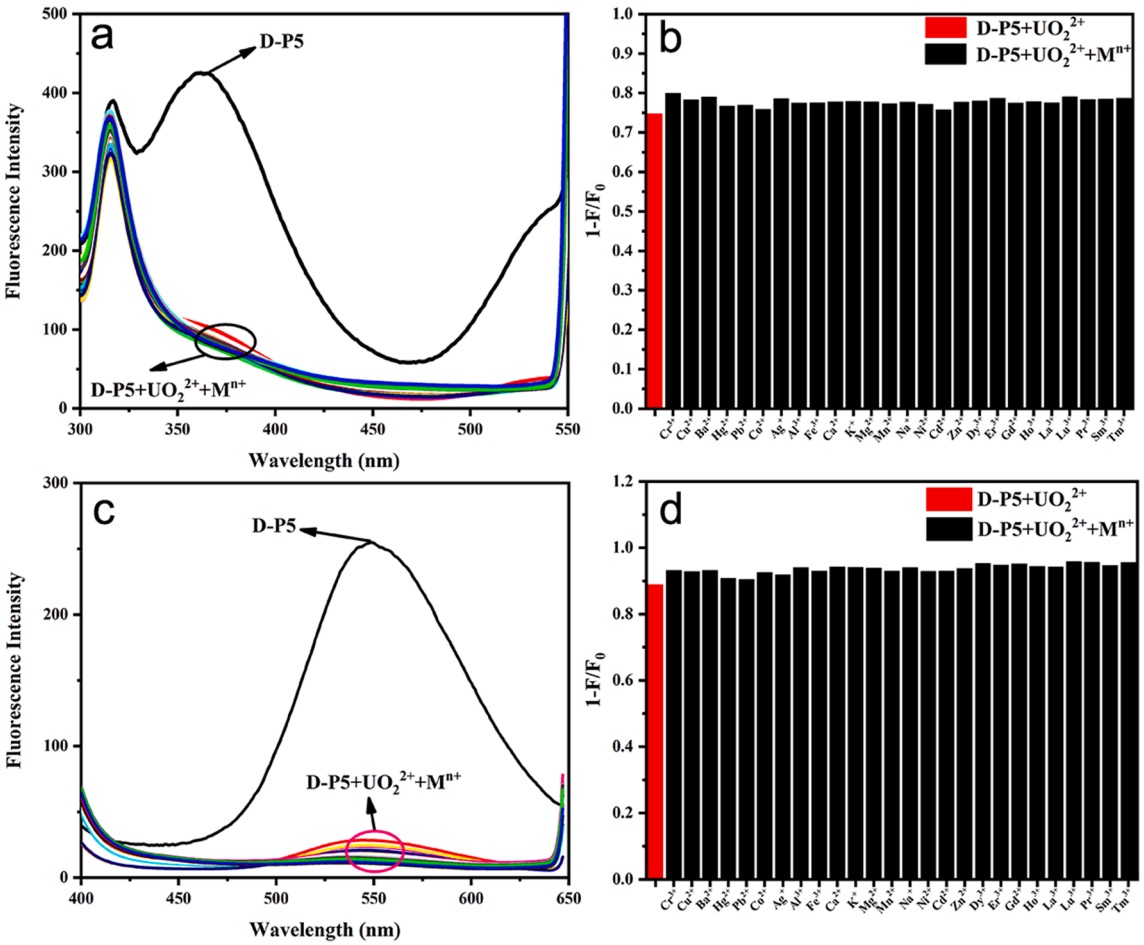

Fig. 2. Fluorescence spectra of D-P5 in the presence of UO_2^{2+} and coexisting metal ions, $\lambda_{ex} = 280$ nm (a) and 330 nm (c). Fluorescence responses of D-P5 to UO_2^{2+} and coexisting metal ions, $\lambda_{ex} = 280$ nm (b) and 330 nm (d). Metal ions concentrations were 30 μM, D-P5 concentration was 10 μM.

2.5. Measurement of detection limit and quantification limit for UO_2^{2+}

For the calculation of the detection limit and the limit of quantification (LOQ) for UO_2^{2+}, their data were obtained from the fluorescence titration experiment by the following formula [32]:

$$LOD = 3SD/m$$

$$LOQ = 10SD/m$$

where *SD* represents relative standard deviation of the blank and *m* represents the slope of the linear fitting line.

2.6. Isothermal titration calorimetry (ITC) measurement

ITC experiment was measured on a MicroCal ITC_{200} titration calorimeter at 298.2 K at the stirring speed of 250 rpm. The reference cell was filled with purified water, and the sample cell was filled with 0.5 mM D-P5 solution. The first injection volume (0.4 μL) was rejected before data analysis. Subsequent titration steps involved 19 injections of 2 μL each of 11 mM UO_2^{2+} solution into the sample cell containing 200 μL D-P5 solution. The duration and interval of each titration were 4 s and 640 s, respectively. Two control experiments were conducted in order to correct for the dilution effects, in which D-P5 solutions were titrated with buffer and the mixture of buffer and UO_2^{2+} solutions, respectively. MicroCal Origin software provided by the ITC_{200} calorimeter was used for all data analyses.

3. Results and discussion

3.1. Fluorescence response of D-P5 to different metal ions

D-P5 fluorescence spectra in the presence of 27 metal ions (UO_2^{2+}, Cr^{3+}, Cu^{2+}, Ba^{2+}, Hg^{2+}, Pb^{2+}, Co^{2+}, Ag^{+}, Fe^{3+}, Ca^{2+}, K^{+}, Mg^{2+}, Mn^{2+}, Na^{+}, Ni^{2+}, Cd^{2+}, Zn^{2+}, Al^{3+}, Dy^{3+}, Er^{3+}, Gd^{2+}, Ho^{3+}, La^{3+}, Lu^{3+}, Pr^{3+}, Sm^{3+}, Tm^{3+}) measured at excitation wavelengths of 280 and 330 nm, respectively, are shown in Fig. 1a and 1c. It could be seen clearly that UO_2^{2+} has a selective and obvious effect on the fluorescence intensity of D-P5. Fig. 1b and 5d show the quenching degree of the D-P5 fluorescence intensity at 360 nm and 550 nm by different metal ions, respectively. The ordinate is $1\text{-}F/F_0$, *F* represents the fluorescence intensity at 360 nm and 550 nm of D-P5 after adding different metal ions, respectively, and F_0 represents the fluorescence intensity of D-P5 itself, which can be found D-P5 can specifically bind to UO_2^{2+} ion.

To further verify the selectivity of D-P5, competitive experiments were performed by adding other metal ions (30 μM) to D-P5 solution (10 μM) in the presence of UO_2^{2+}. As shown in Fig. 2 (a, b, c, d), in the presence of coexisting ions including Cr^{3+}, Cu^{2+}, Ba^{2+}, Hg^{2+}, Pb^{2+}, Co^{2+}, Ag^{+}, Fe^{3+}, Ca^{2+}, K^{+}, Mg^{2+}, Mn^{2+}, Na^{+}, Ni^{2+}, Cd^{2+}, Zn^{2+}, Al^{3+}, Dy^{3+}, Er^{3+}, Gd^{2+}, Ho^{3+}, La^{3+}, Lu^{3+}, Pr^{3+}, Sm^{3+}, Tm^{3+}, the deviations of the fluorescence intensity of D-P5 + UO_2^{2+} were 4.63 % and 4.19 % at the excitation wavelengths of 280 nm and 330 nm, respectively. It can be seen that D-P5 showed higher selectivity to UO_2^{2+} in a competitive environment.

In addition, to further investigated the selectivity of D-P5 sensor for UO_2^{2+}, the fluorescence spectra in the presence of other competitive

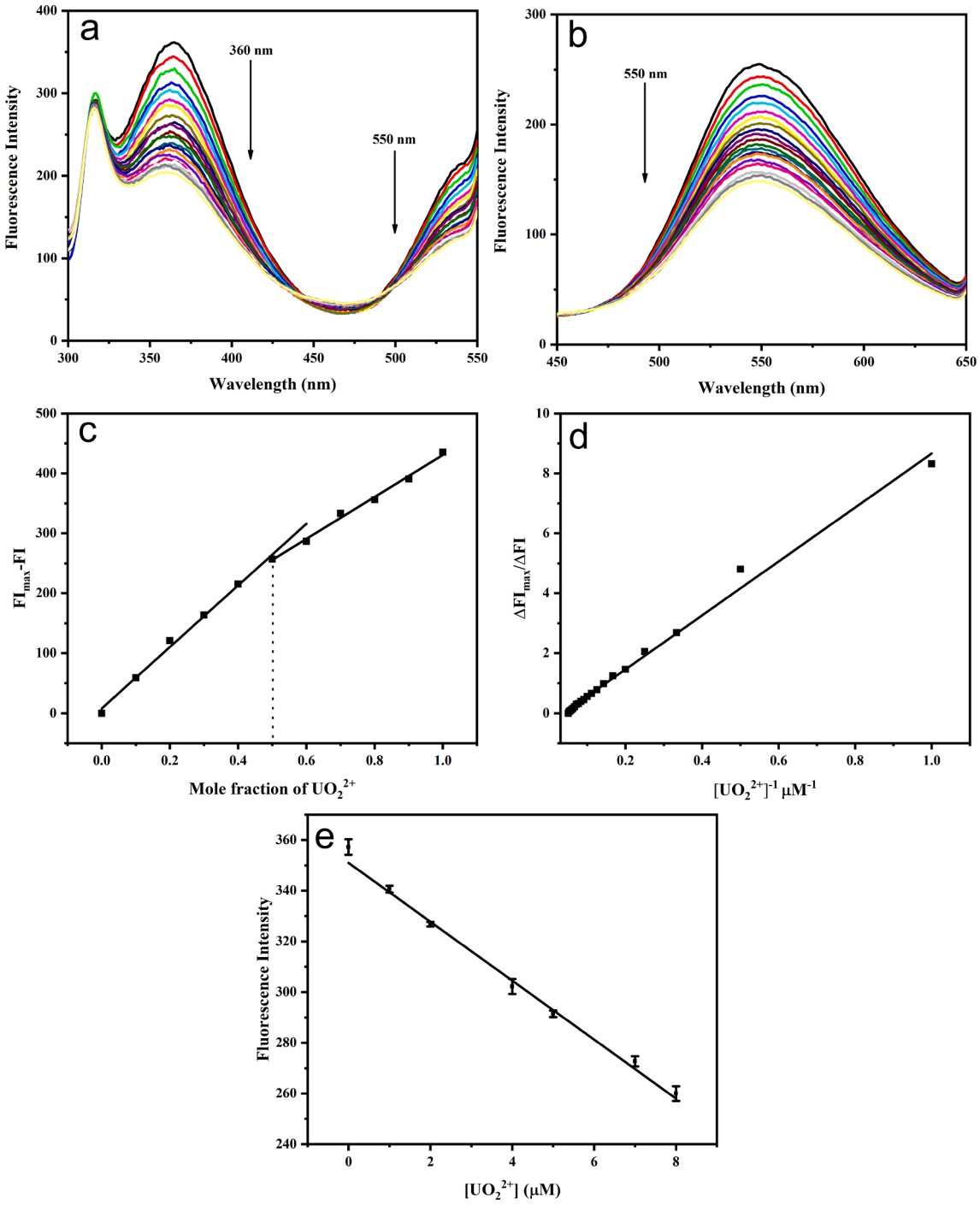

Fig. 3. The fluorescence spectra of D-P5 (10 μM) in the presence of different concentrations of UO_2^{2+} (0–20 μM), λex = 280 nm (a), 330 nm (b); Job's plot curve of the interaction between D-P5 and UO_2^{2+} (c); Benesi-Hildebrand curve of the interaction between D-P5 and UO_2^{2+}(d). The linear relationship between fluorescence intensity of D-P5 (10 μM) and the increased concentration of UO_2^{2+} (c).

species such as some anions ($S_2O_3^{2-}$, S^{2-}, CN^-, SO_4^{2-}, NO_3^-, HSO_4^-, CrO_4^{2-}, HCO_3^-, $HCOO^-$, CH_3COO^-), antioxidant (ascorbic acid) and nitro-aromatic (4-Nitrophenyl acetate) were measured (Fig. S1). Results showed that these species have no obvious effects on the fluorescence of the D-P5 sensor, which further verified that D-P5 can specifically bind to UO_2^{2+}.

In comparison with other methods, the dansyl-modified peptide sensor has some advantages including analytical characteristics, specificity, stability and reproducibility. The dansyl-modified peptide sensor has the advantages of both peptide and fluorescent group Dansyl. Compared with other types of sensors, peptide-based sensors have good water solubility, biocompatibility, and low toxicity, and therefore have important applications in environmental detection and bioanalytical diagnosis. Peptide sensors can achieve specific selectivity to different metal ions by adjusting their sequences because different peptides have different coordination to different metal ions. Dansyl is a strong fluorescent group commonly used in the modification of peptide because it can react specifically with primary amino groups at the *N*-terminal of peptide chain to produce a stable and strong fluorescent sulfonamide adduct of dansyl-peptide. In addition, the synthesized D-P5 sensor has good stability and reproducibility in aqueous solution for detecting UO_2^{2+} ion.

Table 1
Comparison of present work with literature reports.

Ref.	Method of detection	Sensor type	Solution (v/v)	Detection limit (nM)	Binding constant
[15]	Fluorescence	Conjugated polymer	DMA: H_2O = 20:80	7.4	1.11×10^6
[33]	UV–vis	Nanomaterial	H_2O	500	–
[16]	Fluorescence	Small molecule	DMSO	41	9.4×10^5
[25]	Fluorescence	phosphorylated cyclic peptide	MES	360	2.4×10^5
[3]	Fluorescence	Small molecule	THF:H_2O = 5:95	50	–
This work	Fluorescence	Short peptide	HEPES	83.2	9.8×10^4

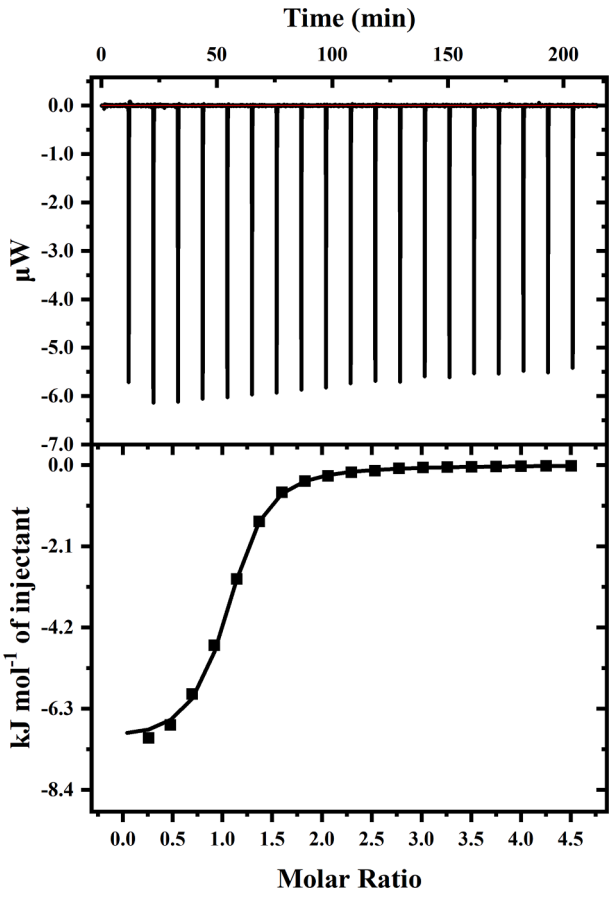

Fig. 4. ITC profiles for the binding of D-P5 to UO_2^{2+} at 298.2 K. The upper and lower panels represent the raw data for the titration of successive aliquots of UO_2^{2+} into D-P5 solution and the integrated heat after correction of the dilution heat, respectively.

3.2. Binding stoichiometry, binding constant, detection limit and quantification limit

The variations of D-P5 fluorescence intensity with increasing concentration of UO_2^{2+} (1.0–20.0 μM) in 10.0 mM HEPES buffer (pH 6.3) were determined by the fluorescence titration experiments. As shown in Fig. 3a and 3b, the fluorescence intensity of D-P5 decreased with UO_2^{2+} concentration increasing, indicating that the coordination of UO_2^{2+} with D-P5 led to a rapid fluorescence quenching.

The stoichiometric ratio between the sensor D-P5 and UO_2^{2+} was determined according to Job's plot. Fig. 3c shows that the D-P5:UO_2^{2+} binding ratio was 1:1. The binding constant of UO_2^{2+} to D-P5 was calculated by the modified Benesi-Hildebrand equation (Fig. 3d). The binding constant was calculated to be 9.8×10^4 M^{-1} (R^2 = 0.99227), which means that D-P5 had a strong binding affinity to UO_2^{2+}.

The detection limit and quantification limit were measured based the fluorescence titration experiment at excitation wavelengths of 280 nm, the fluorescence intensity of D-P5 was linearly related to the concentration of UO_2^{2+}. The detection limit and quantification limit were calculated to be 83.2 nM and 277.3 nM (R^2 = 0.99338) from the formula $LOD = 3SD/m$ and $LOQ = 10SD/m$, respectively (Fig. 3e). The result indicated that D-P5 has a high sensitivity for UO_2^{2+} detection. Table 1 lists some other sensors for the detection of uranyl ion for comparison, indicating that D-P5 is a highly selective and sensitive fluorescence sensor for UO_2^{2+} in the water solution.

3.3. Isothermal titration calorimetry (ITC) study

ITC is one of the most direct methods to measure the thermal effect of ligand–protein interaction. Using this method, the binding constant, the number of binding site and the enthalpy change can be determined simultaneously for their interaction [34]. ITC profiles for the binding of D-P5 to UO_2^{2+} are shown in Fig. 4. The enthalpy change ΔH^θ and entropy change ΔS^θ for the interaction of D-P5 with UO_2^{2+} were $-(7.167 \pm 1.25)$ kJ·mol^{-1} and 66.5 J·mol^{-1}·K^{-1}, respectively. The binding constant K obtained by fitting method was $5.32 \times 10^4 \pm 250$ M^{-1}, indicating again that D-P5 has a good binding ability to UO_2^{2+}.

3.4. Characterization analysis for the binding of D-P5 with UO_2^{2+}

3.4.1. ESI-MS

ESI-MS analysis was set in the positive ion mode. Fig. 5 is the ESI-MS of D-P5 and D-P5 + UO_2^{2+}. The successful synthesis was confirmed by ESI-MS. ESI mass of D-P5 is calculated as 922.3 [M + H^+]. Observed 922.3 as [M + H^+], 966.3 as [(M−2H^+) + 2Na^++H^+] and 1028.3 as [(M−3H^+) + K^++3Na^+] (Fig. 5a). Fig. 5b shows the ESI-MS result of D-P5 + UO_2^{2+}, it was found that the occurrences of peak 1190.3 and 1223.8 correspond to [(M−2H^+) + UO_2^{2+}+H^+] and [(M−3H^+) + UO_2^{2+}+2NH_4^+], respectively. These results confirmed that D-P5 could bind to UO_2^{2+} in the ratio of 1:1 to form D-P5 + UO_2^{2+} complex.

3.4.2. FT-IR

FTIR spectral study was conducted to investigate which chemical groups of D-P5 played a vital role in the interaction with UO_2^{2+}. Fig. 6a shows the IR spectra of D-P5 and D-P5 + UO_2^{2+}. The IR peaks at 3413.39 and 3067.47 cm^{-1} can be attributed to N—H and the O—H stretching vibrations in D-P5. The IR peaks at 1721.49 cm^{-1} and 1669.62 cm^{-1} were the characteristic absorption peaks of C═O groups in amide bond and carboxylic acid group, respectively. The peaks at 2360.25 and 2956.34 cm^{-1} are corresponding to stretching vibrations of O═S = O and C—H. The IR spectrum of D-P5 in the 1201.24–1516.34 cm^{-1} region can be attributed to C—H deformation as well as C—N and C—S stretching vibrations. After adding UO_2^{2+} to the D-P5 solution, the peak at 3413.39 cm^{-1} shifted to 3407.95 cm^{-1} and 3067.47 cm^{-1} and almost disappeared, indicating that the N—H and the O—H groups involved in the interaction with UO_2^{2+}. Further, the peak shape changed and the intensity significantly reduced for the bands of 1721.49 cm^{-1} and 1669.62 cm^{-1}, which also proved that the carboxyl group of Glu and the amide group interacted with UO_2^{2+} [35,36]. In addition, compared with D-P5 itself, the peak at 936.08 cm^{-1} in D-P5 + UO_2^{2+} should be attributed to the stretching vibration of the O = U = O, which further proved that UO_2^{2+} was bound to D-P5 [22,37].

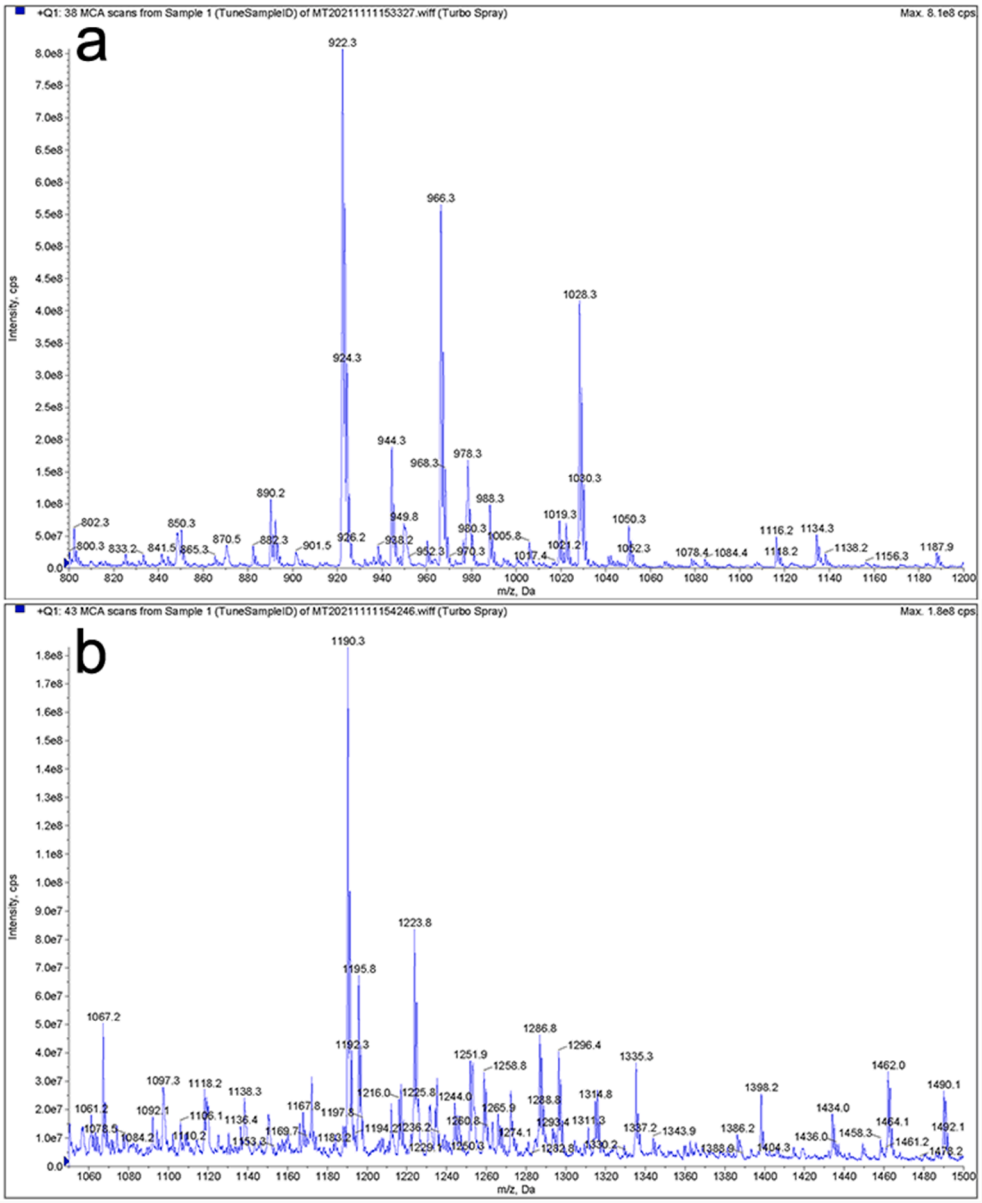

Fig. 5. ESI mass spectra of D-P5 (a) and D-P5 + UO_2^{2+} (b).

3.4.3. XPS

The XPS measurement was used to further explore which elements and chemical bonds existed in the interaction of the sensor D-P5 with UO_2^{2+}. As shown in Fig. 6b-e, XPS spectra of C1s, O1s and N1s of D-P5 and D-P5 + UO_2^{2+} were measured, and the obtained spectra were fitted with peaks by Avantage software. Tables S1-3 show the specific peaks splitting situation of the binding energy obtained of C1s, N1s, and O1s.

By fitting the C 1 s peaks of D-P5 and D-P5 + UO_2^{2+} (Fig. 6c), it can be concluded that the main forms of C element in D-P5 are C—C, COOH, O═C-N. The C 1 s of D-P5 + UO_2^{2+} was nearly the same as that of D-P5, speculating that C in the peptide does not interact with UO_2^{2+}. As shown in Fig. 6d, a fitting analysis was performed for the N1s peak. Compared with the N1s of D-P5, a new peak at 400.14 eV was found in that of D-P5 + UO_2^{2+}, which could be assigned to U-N and demonstrate the coordination of D-P5 with UO_2^{2+} [38,39]. After adding UO_2^{2+}, O═C-N peak shifted from 399.25 eV to 399.27 eV [40], which originates from the electron cloud density and the outer electrons of the N atom attracted by the uranyl cation, resulting in a relatively high bond energy. It can be inferred that the N element of the amide bond in the peptide interacted with UO_2^{2+}. In Fig. 6e, the O1s XPS spectrum of D-P5 can be divided into three overlapping peaks, which locate at 531.27 eV, 532.45 eV and 533.70 eV and can be assigned to COO^-, O═C-NH- and O═C, respectively. After adding UO_2^{2+}, the three peaks of COO^-, O═C-NH- and O═C are shifted to 531.50 eV, 532.21 eV and 533.38 eV, which indicated that the carboxyl of D-P5 also interacted with UO_2^{2+} [41–43]. Compared with the XPS spectra of the $UO_2(NO_3)_2{\cdot}6H_2O$, the binding energy of U 4f was obviously decreased in D-P5 + UO_2^{2+} (inset in Fig. 6f), suggesting that the electron density of the U atom increased [44]. The U 4f core level was further deconvoluted into two doublets, which were attributed to U $4f_{7/2}$ and U $4f_{5/2}$. The U4f spectrum was fitted and analyzed according to the previous work, which were attributed to U-O. In the fitted spectra, the higher binding energy (385.82 eV and 393.67 eV) may be due to the coordination of U-N or U-S. But according to the change in the spectrum of N1s (Fig. 6d), we speculated that these peaks are more in line with the characteristics of U-N coordination [45].

3.4.4. Time-resolved fluorescence spectroscopy

To obtain the accurate information about the quenching mechanisms, the time-resolved fluorescence spectroscopy for D-P5 and D-P5 + UO_2^{2+} were performed by FLS 1000 Photoluminescence Spectrometer.

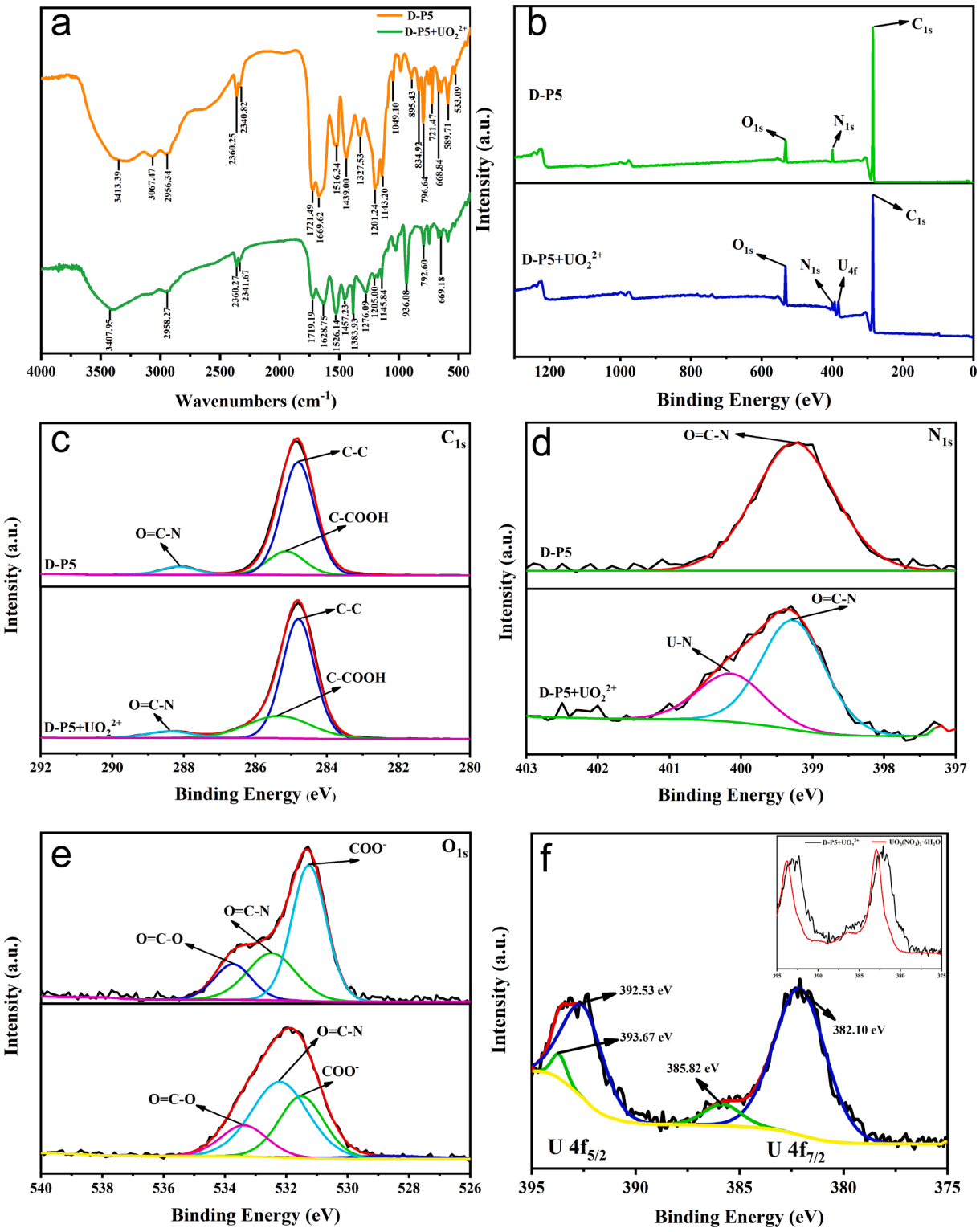

Fig. 6. FT-IR spectra of D-P5 (orange) and D-P5 + UO_2^{2+} (green) (a). XPS spectra of D-P5 and D-P5 + UO_2^{2+} (b), C1s (c), N1s (d), and O1s (e). XPS spectra of U 4f for D-P5 + UO_2^{2+} (f) (Inset: comparision of XPS spectra of U 4f for D-P5 + UO_2^{2+} with that for $UO_2(NO_3)_2{\cdot}6H_2O$). (For interpretation of the references to colour in this figure legend, the reader is referred to the web version of this article.)

Fig. 7 is the fluorescence lifetime decay profiles excited at 280 nm (a) 330 nm (b) for D-P5 and D-P5 + UO_2^{2+} in 10 mM Hepes buffer (pH 6.3). As shown in Fig. 7, under the excitation wavelength of tryptophan residues (a, 280 nm) and dansyl groups (b, 330 nm), the curves of the samples before and after the addition of UO_2^{2+} did not change significantly. The fitting formula of fluorescence lifetime curve was given by the instrument: $R(t) = B_1e^{(-t/\tau 1)} + B_2e^{(-t/\tau 2)}$, and the obtained data were analyzed (Tables S4 and S5). From Tables S4 and S5, it can be seen that the slower and faster decay components (B1, B2) of Trp and dansyl had no obvious changes before and after adding UO_2^{2+}. The corresponding average lifetimes can be calculated by the formula $[\tau] = \sum \tau_i \cdot B_i$. It is found that the average fluorescence lifetime of Trp residue of D-P5

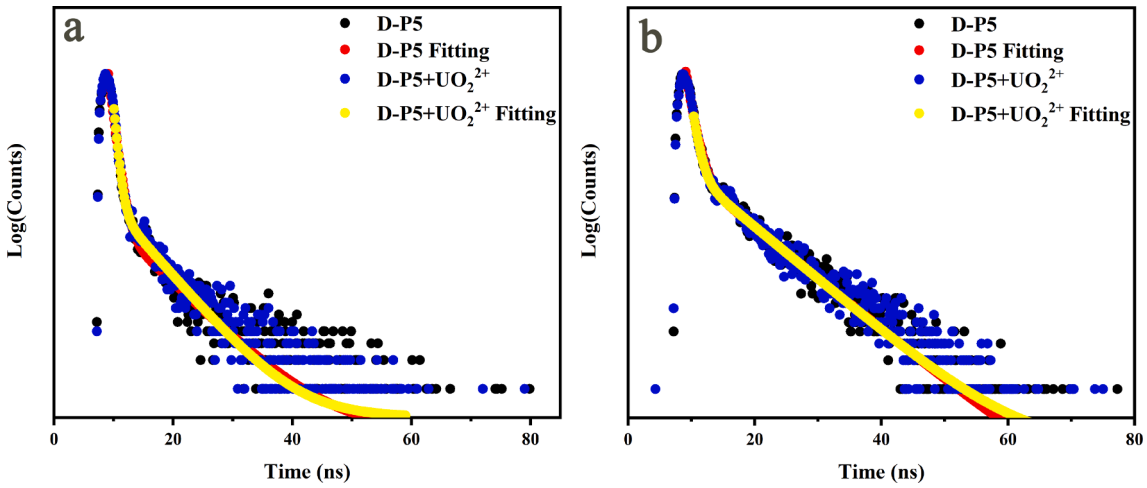

Fig. 7. Fluorescence lifetime decay profiles excited at 280 nm (a) 330 nm (b) for D-P5 (10.0 μM) and D-P5 + UO_2^{2+} (10.0 μM) in buffer (pH 6.3, 10 mM Hepes).

Table 2
Detection of UO_2^{2+} in lake water and ICP-MS detection the concentration of UO_2^{2+}.

UO_2^{2+} added		UO_2^{2+}found		Recovery (%)		RSD(%, n = 3)	
This method (μM)	ICP-MS (ppb)	This method (μM)	ICP-MS (ppb)	This method	ICP-MS	This method	ICP-MS
2.0	10.0	2.1 (±0.06)	10.4	105	104	2.8	1.5
3.0	15.0	2.8 (±0.06)	15.5	93	103	2.0	1.4
5.0	25.0	4.9 (±0.06)	24.5	98	98	1.1	1.7
7.0	35.0	6.9 (±0.15)	36.0	99	103	2.2	2.0

sensor decreased a little after adding UO_2^{2+}, but the average fluorescence lifetimes of dansyl group did not change. The result showed that the mechanism of fluorescence quenching by UO_2^{2+} ion was static quenching process [10,12,46]. The effect of UO_2^{2+} on the fluorescence lifetime of tryptophan residue could be explained as follows. In the quenching process, firstly, the interaction between UO_2^{2+} and D-P5 may lead to the distortion of the planarity of indole ring in Trp residue, thus changing the local environment around Trp residue, and resulting a little decrease of fluorescence lifetime of Trp residue.

And the radiation rate constant (k_r) and the non-radiation rate constant (k_{nr}) are obtained by the following formula [11,47]:

$$k_r = Q/[\tau]$$

$$k_{nr} = 1/(Q\cdot[\tau])$$

Where Q represents quantum yield and $[\tau]$ represents average fluorescence lifetime.

The obtained radiation rate constants (k_r) and non-radiation rate constants (k_{nr}) are listed in Tables S6 and S7, it can be seen that the k_r values both of tryptophan residue and dansyl group in D-P5 decreased when UO_2^{2+} ions were added, which was due to the increase of polarity of tryptophan residue and dansyl microenvironment after adding of UO_2^{2+}. However, their corresponding k_{nr} rate constants increased when UO_2^{2+} was added, which showed that the D-P5 sensor interacted with UO_2^{2+}.

3.5. Application for detection of UO_2^{2+} in lake water samples

In order to explore the application of D-P5 fluorescence sensor for detecting UO_2^{2+} in real samples, we measured UO_2^{2+} in lake water. First, we used distilled water to prepare standard samples of UO_2^{2+}, measured their fluorescence spectra and obtained a standard curve (0–8 μM) according to the concentration gradient. Then, we used lake water to prepare UO_2^{2+} solutions with concentrations of 2, 3, 5 and 7 μM. Fluorescence measurements were performed separately, and the obtained fluorescence intensity was used to calculate the concentration of UO_2^{2+} through the standard curve equation. To evaluate the statistical analysis for determination results, we also measured UO_2^{2+} in lake water by ICP-MS, a typical method for detecting UO_2^{2+}. The results are shown in Table 2. Compared with ICP-MS method, the relative standard deviation (RSD) and the recovery rates of D-P5 sensor are similar for UO_2^{2+} detection in lake water. Importantly, D-P5 sensor is a simple, sensitive and selective method for the determination of UO_2^{2+} in real sample. Therefore, D-P5 can be used as a good potential sensor for environmental detection of UO_2^{2+} in water sample.

4. Conclusion

In summary, a novel dansyl-modified peptide fluorescence sensor (D-P5) has been synthesized for the detection of uranyl ion. As far as we know, it is the first linear peptide-based sensor of UO_2^{2+}. The sensor displayed a turn-off fluorescence response mode for highly selective detection of UO_2^{2+}. Among the common metal ions and rare earth metal ions in 10 mM HEPES buffer solution, D-P5 sensor exhibited specific and high affinity to UO_2^{2+} ion with a binding constant of 9.8×10^4 M^{-1}. The sensor showed highly selective and sensitive to UO_2^{2+}, and its detection limit and quantification limit for UO_2^{2+} ion were estimated as low as 83.2 nM and 277.3 nM, respectively. Furthermore, the interaction of D-P5 with UO_2^{2+} was investigated by IR, ESI-MS, XPS and ITC measurements. The fluorescence static quenching mechanism of D-P5 by UO_2^{2+} ion was inferred by time-resolved fluorescence spectroscopy study. In addition, this sensor was successfully used to detect UO_2^{2+} ion in lake water sample, indicating its great potential in practical use for the detection of UO_2^{2+} ion. More importantly, although the detection limit of the peptide-based UO_2^{2+} fluorescence sensor still has a certain gap compared with some organic compound fluorescence sensors, it is the first report on the linear peptide-based fluorescence sensor, which has some excellent advantages of peptide. Therefore, this sensor shows great potential in the applications in biological and environmental systems.

CRediT authorship contribution statement

Lianshun Zhang: Conceptualization, Investigation, Methodology, Data curation, Writing – original draft. **Mengqing Jia:** Investigation. **Xi**

Wang: Investigation. **Lei Gao:** Investigation. **Bo Zhang:** Supervision. **Lei Wang:** Investigation, Formal analysis, Supervision. **Jinming Kong:** Supervision, Funding acquisition, Writing – review & editing. **Lianzhi Li:** Conceptualization, Supervision, Funding acquisition, Writing – review & editing.

Declaration of Competing Interest

The authors declare that they have no known competing financial interests or personal relationships that could have appeared to influence the work reported in this paper.

Data availability

Data will be made available on request.

Acknowledgements

This work was supported by the Scientific Research Foundation of Liaocheng University, China (No. 318011919), and the National Natural Science Foundation of China (No. 21974068).

Appendix A. Supplementary material

Supplementary data to this article can be found online at https://doi.org/10.1016/j.saa.2023.122403.

References

[1] G. Schreckenbach, S.K. Wolff, T. Ziegler, NMR shielding calculations across the periodic table: diamagnetic uranium compounds. 1. methods and issues, J. Phys. Chem. A 104 (2000) 8244–8255.
[2] Z. Tosheva, K. Stoyanova, L. Nikolchev, Comparison of different methods for uranium determination in water, J. Environ. Radioactiv. 72 (2004) 47–55.
[3] M. Zheng, Q. Yin, D.Y. Wang, Z.X. Zhao, Q.H. Hu, H.Q. Wang, A fluorescent probe of uranyl for acid and high water system and imaging in living cells, Microchem. J. 167 (2021), 106302.
[4] G. Bjørklund, Y. Semenova, L. Pivina, M. Dadar, M. Rahman, J. Aaseth, S. Chirumbolo, Uranium in drinking water: a public health threat, Arch. Toxicol. 94 (2020) 1551–1560.
[5] B. Peng, X.Y. Tang, X. Yu, S.R. Xie, M.L. Xiao, Z. Song, X.L. Tu, Heavy metal geochemistry of the acid mine drainage discharged from the Hejiacun uranium mine in central Hunan, China, Environ. Geol. 57 (2009) 421–434.
[6] J.H. Lee, Z.D. Wang, J.W. Liu, Y. Lu, Highly sensitive and selective colorimetric sensors for uranyl (UO_2^{2+}): Development and comparison of labeled and label-free DNAzyme-Gold Nanoparticle systems, J. Am. Chem. Soc. 130 (2008) 14217–14226.
[7] S.C. Yang, S.Y. Jiang, K. Hu, X.D. Wen, Investigation of dispersive solid-phase extraction combined with slurry sampling thermospray flame furnace atomic absorption spectrometry for the determination of cadmium, Microchem. J. 154 (2020), 104542.
[8] D.W. Boomer, M.J. Powell, Determination of uranium in environmental samples using inductively coupled plasma mass spectrometry, Anal. Chem. 59 (1987) 2810–2813.
[9] C. Pin, J.S. Zalduegui, Sequential separation of light rare-earth elements, thorium and uranium by miniaturized extraction chromatography: Application to isotopic analyses of silicate rocks, Anal. Chim. Acta 339 (1997) 79–89.
[10] S.O. Tümay, V. Şanko, A. Şenocak, E. Demirbas, A hybrid nanosensor based on novel fluorescent iron oxide nanoparticles for highly selective determination of Hg^{2+} ions in environmental samples, New. J. Chem. 45 (2021) 14495–14507.
[11] S.O. Tümay, A. Şenocak, A. Mermer, A "turn-on" small molecule fluorescent sensor for the determination of Al^{3+} ion in real samples: theoretical calculations, and photophysical and electrochemical properties, New. J. Chem. 45 (2021) 18400–18411.
[12] S.O. Tümay, A novel selective "Turn-On" fluorescent chemosensor based on thiophene appended cyclotriphosphazene schiff base for detection of Ag^+ ions, ChemistrySelect 6 (2021) 10480–10733.
[13] N. Lin, W. Ren, J. Hu, B. Gao, D. Yuan, X. Wang, J. Fu, A novel tetraphenylethene-based fluorescent sensor for uranyl ion detection, with aggregation-induced emission character, Dyes Pigments 166 (2019) 182–188.
[14] N. Lin, R. Tao, Z.J. Chen, Q.F. Pan, Z.H. Zhu, B. Gao, W.S. Ren, Design and fabrication of a new fluorescent film sensor towards uranyl ion via self-assembled monolayer, J. Lumin. 242 (2022), 118562.
[15] Q.H. Hu, W.F. Zhang, Q. Yin, Y.Y. Wang, H.Q. Wang, A conjugated fluorescent polymer sensor with amidoxime and polyfluorene entities for effective detection of uranyl ion in real samples, Spectrochim. Acta A 244 (2021), 118864.
[16] A.A. Elabd, M.S. Attia, A new thin film optical sensor for assessment of UO_2^{2+} based on the fluorescence quenching of trimetazidine doped in sol gel matrix, J. Lumin. 165 (2015) 179–184.
[17] C.R. Zhang, W.R. Cui, W. Jiang, F.F. Li, Y.D. Wu, R.P. Liang, J.D. Qiu, Simultaneous sensitive detection and rapid adsorption of UO22+ based on a post-modified sp2 carbon-conjugated covalent organic framework, Environ. Nano 7 (2020) 842–850.
[18] A.A. Elabd, M.S. Attia, Spectroflourimetric assessment of UO_2^{2+} by the quenching of the fluorescence intensity of clopidogrel embedded in PMMA matrix, J. Lumin. 169 (2016) 313–318.
[19] Q.T. Liu, J.F. Wang, B.J. Boyd, Peptide-based biosensors, Talanta 136 (2015) 114–127.
[20] F. Brulfert, S. Safi, A. Jeanson, E. Martinez-Baez, J. Roques, C. Berthomieu, P. L. Solari, S. Sauge-Merle, É. Simoni, Structural environment and stability of the complexes formed between calmodulin and actinyl ions, Inorg. Chem. 55 (2016) 2728–2736.
[21] C. Lebrun, M. Starck, V. Gathu, Y. Chenavier, P. Delangle, Engineering short peptide sequences for uranyl binding, Chem. Eur. J. 20 (2014) 16566–16573.
[22] G.A. Senchyka, A.B. Lysenko, H. Krautscheid, K.V. Domasevitcha, Control over the coordination preferences in Ag^+ and Ag^+/UO_2^{2+} 1,2,4-triazolecarboxylate frameworks, Inorg. Chem. Commun. 113 (2020), 107813.
[23] I. Feldman, L. Koval, Reaction of the uranyl ion with amino acids. bidentate carboxylate chelation, Inorg. Chem. 2 (1963) 145–150.
[24] Q.Y. Wu, J.H. Lan, C.Z. Wang, C.L. Xiao, Y.L. Zhao, Y.Z. Wei, Z.F. Chai, W.Q. Shi, Understanding the bonding nature of uranyl ion and functionalized graphene: A Theoretical Study, J. Phys. Chem. A 118 (2014) 2149–2158.
[25] C.T. Yang, J. Han, M. Gu, J. Liu, Y. Li, Z. Huang, H.Z. Yu, S. Hu, X.L. Wang, Fluorescent recognition of uranyl ions by a phosphorylated cyclic peptide, Chem. Commun. 51 (2015) 11769–11772.
[26] L.L. Clainche, C. Vita, Selective binding of uranyl cation by a novel calmodulin peptide, Environ. Chem. Lett. 4 (2006) 45–49.
[27] A. Trapaidze, C. Hureau, W. Bal, M. Winterhalter, P. Faller, Thermodynamic study of Cu^{2+} binding to the DAHK and GHK peptides by isothermal titration calorimetry (ITC) with the weaker competitor glycine, J. Biol. Inorg. Chem. 17 (2012) 37–47.
[28] H. Huang, S. Chaudhary, J.D. Van Horn, Uranyl-Peptide interactions in carbonate solution with DAHK and derivatives, Inorg. Chem. 44 (2005) 813–815.
[29] P.F. Mühlradt, M. Kieß, H. Meyer, R. Sümuth, G. Jung, Isolation, structure elucidation, and synthesis of a macrophage stimulatory lipopeptide from mycoplasma fermentans acting at picomolar concentration, J. Exp. Med. 185 (1997) 1951–1958.
[30] S. Das, A. Sahana, A. Banerjee, S. Lohar, D.A. Safin, M.G. Babashkina, M. Bolte, Y. Garcia, I. Hauli, S.K. Mukhopadhyay, D. Das, Ratiometric fluorescence sensing and intracellular imaging of Al^{3+} ions driven by an intramolecular excimer formation of a pyrimidine-pyrene scaffold, Dalton. T. 42 (2013) 4753–4757.
[31] S. Sarkar, S. Roy, R.N. Saha, S.S. Panja, Thiophene appended dual fluorescent sensor for detection of Hg^{2+} and cysteamine, J. Fluoresc. 28 (2018) 427–437.
[32] S.B. Yu, Y. Li, L. Gao, P.R. Zhao, L. Wang, L.Z. Li, Y.W. Lin, A highly selective and sensitive Zn^{2+} fluorescent sensor based on zinc finger-like peptide and its application in cell imaging, Spectrochim. Acta. A 261 (2021), 120042.
[33] L. Yun, H. Yi, Arsenazo III-functionalized gold nanoparticles for photometric determination of uranyl ion, Microchim. Acta 183 (2016) 407–413.
[34] A. Basu, G.S. Kumar, Interaction of the dietary pigment curcumin with hemoglobin: Energetics of the complexation, Food Funct. 5 (2014) 1949–1955.
[35] W. Chin, F. Piuzzi, J.P. Dognon, I. Dimicoli, B. Tardivel, M. Mons, Gas phase formation of a 3_{10}-Helix in a three-residue peptide chain: Role of side chain-backbone interactions as evidenced by IR−UV double resonance experiments, J. Am. Chem. Soc. 127 (2005) 11900–11901.
[36] J. Yu, X.G. Luo, B. Liu, J. Zhou, J. Feng, W.K. Zhu, S.L. Wang, Y.D. Zhang, X.Y. Lin, P. Chen, Bayberry tannin immobilized bovine serum albumin nanospheres: characterization, irradiation stability and selective removal of uranyl ions from radioactive wastewater, J. Mater. Chem. A 6 (2018) 15359–15370.
[37] S. Park, J. Park, J.H. Lee, M.Y. Choi, J.H. Jung, Spectroscopic study of the salicyladazine derivative–UO_2^{2+} complex and its immobilization to mesoporous silica, Nanomaterials 9 (2019) 688.
[38] J.S. Stevens, A.C. Luca, M. Pelendritis, G. Terenghi, S. Downes, S.L.M. Schroeder, Quantitative analysis of complex amino acids and RGD peptides by X-ray photoelectron spectroscopy (XPS), Surf. Interface. Anal. 45 (2013) 1238–1246.
[39] Y. Cho, A. Ivanisevic, TAT Peptide Immobilization on Gold Surfaces: A Comparison Study with a Thiolated Peptide and Alkylthiols Using AFM, XPS, and FT-IRRAS, J. Phys. Chem. B 109 (2005) 6225–6232.
[40] C.M. Whelan, F. Cecchet, R. Baxter, F. Zerbetto, G.J. Clarkson, D.A. Leigh, P. Rudolf, Adsorption of a benzylic amide macrocycle on a solid substrate: XPS and HREELS characterization of thin films grown on Au(111), J. Phys. Chem. B 106 (2002) 8739–8746.
[41] S.V. Berghea, J.P. Laval, B. Gaudreaub, H. Terrync, M. Verwerft, XPS investigations on cesium uranates: mixed valency behaviour of uranium, J. Nucl. Mater. 277 (2000) 28–36.
[42] S. Bera, S.K. Sali, S. Sampath, S.V. Narasimhan, V. Venugopal, Oxidation state of uranium: an XPS study of alkali and alkaline earth uranates, J. Nucl. Mater. 255 (1998) 26–33.
[43] A. Froideval, M. Del Nero, R. Barillon, J. Hommet, G. Mignot, pH dependence of uranyl retention in a quartz/solution system: an XPS study, J. Colloid. Interf. Sci. 266 (2003) 221–235.
[44] X. Lu, D. Zhang, A.T. Reda, C. Liu, Z. Yang, S. Guo, S. Xiao, Y. Ouyang, Synthesis of amidoxime-grafted activated carbon fibers for efficient recovery of uranium(VI) from aqueous solution, Ind. Eng. Chem. Res. 56 (2017) 11936–11947.

[45] Y.Y. Gao, Q. Zhang, Y. Lv, S. Wang, M. Men, H. Kobayashi, Z.L. Xu, Y. Wang, Peptide-carbon hybrid membranes for highly efficient and selective extraction of actinides from rare earth elements, J. Mater. Chem. A 9 (2021) 14422–14431.
[46] H. İbişoğlu, Z. Kılıç, F. Yuksel, S.O. Tümay, Synthesis, characterization, photophysical and intramolecular energy transfer properties of oxy-naphthylchalcone appended cyclotriphosphazene cores, J. Lumin. 222 (2020), 117125.
[47] J.R. Albani, Relation between the secondary structure of carbohydrate residues of α_1-acid glycoprotein (orosomucoid) and the fluorescence of the protein, Carbohyd. Res. 338 (2003) 1097–1101.